ID-1005

STRENGTHENING OF REINFORCED CONCRETE NUCLEAR REACTOR CONTAINMENT WITH FIBER COMPOSITE LAMINATE MATERIALS

Hsuan-Teh Hu and Te-Fu Chou

Department of Civil Engineering, National Cheng Kung University, Tainan, Taiwan, China

SUMMARY: Numerical analyses are performed by using the ABAQUS finite element program to predict the ultimate pressure capacity of the reinforced concrete containment strengthened by composite materials or steel plates at various positions. Material nonlinear behaviors related to concrete, steel and fiber composite laminate material are all simulated with proper constitutive models. It has been shown that the uses of $[\pm\theta/90/0]_{5S}$ composite materials with $50^{O} \le \theta \le 90^{O}$ to strengthen the containment at the upper cylinder and the dome simultaneously achieve the most satisfactory strengthening results.

KEYWARDS: Strengthen, Reinforced Concrete Containment, Composite Materials

INTRODUCTION

The reinforced concrete nuclear reactor containments at Taiwan were built in the late 70's and the design life cycle is 40 years. It is known that the mechanical properties of the containment materials degrade as time elapses. Consequently, after a long-term service, the ultimate pressure strength of the containment would be lower than the initial design value and the strengthening of the containment structure may become necessary. The traditional material used in strengthening of concrete structures is the steel. Because of its drawbacks of low corrosion resistance, excessive size and weight, there is a need for the engineering community to look for alternatives. Due to lightweight, high strength and good fatigue and corrosion properties, composite materials have been intensively used in the repairing and strengthening of aerospace structures [1]. Though, the study of using composite materials to strengthen the reinforced concrete structures just started in 90's [2], it is feasible to use the technology in the near future. In the paper, finite element program ABAQUS [3] is used to perform the ultimate analysis of the reinforced concrete containment, strengthened by steel plates or fiber composite laminate materials, at Kuosheng nuclear power plant. The geometry and finite element mesh of the containment are reviewed first. Then, material properties of reinforcing steel, liner plate, strengthening steel plate, concrete and composite material are given and proper constitutive models are introduced to simulate their nonlinear behaviors. Finally, failure analyses of the reinforced concrete containment strengthened by steel plates or composite materials at various positions and subjected to internal pressure are carried out and important conclusions are given.

CONTAINMENT GEOMETRY AND FINITE ELEMENT MESH

The reinforced concrete containment at Kuosheng Nuclear Power Plant is composed of a circular base slab, an upright cylinder and a hemispherical dome (Fig. 1). To simplify the analysis, equipment hatches and penetrations on the containment are not considered and

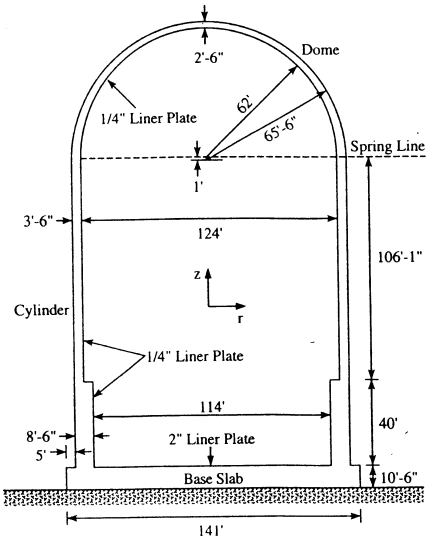

Fig. 1 Geometry of containment

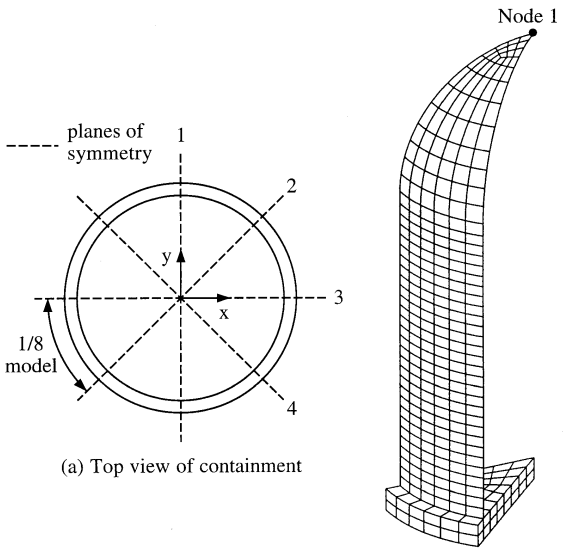

Fig. 2 1/8 model of the containment

the structure geometry is assumed to be axisymmetric. The entire interior surface of the dome, cylinder and base slab are lined with continuous steel plate system to provide a leak-tight barrier. The thickness of the steel liner plate inside the dome and cylinder is 0.635 cm (1/4") while the thickness of the steel plate on the base slab is 5.08 cm (2"). Most of the steel reinforcing bars are placed in an axisymmetric manner in the containment and the detailed arrangements of steel reinforcing bars are given in the Final Safety Analysis Report of the Kuosheng nuclear power plant [4]. Because some steel reinforcement layers in the base slab are placed in the directions parallel to x and y axes, the deformation of the containment will no longer be axisymmetric and will have four planes of symmetry (Fig. 2). As a result, only 1/8 part of the structure is analyzed and symmetric boundary conditions are imposed on the symmetric planes. In the numerical simulation, 8-node shell elements are used to model the parts of dome and cylinder, and 27-node solid elements are used to model the base slab. The liner plates are also modeled by the 8-node shell elements. They are either linked to the shell elements of the concrete section at the parts of dome and cylinder, or attached to the inner surface of the solid elements at the base slab. At the bottom of the base slab, special purpose 9-node interface elements are used to link the base slab to the ground. The interface elements allow the contact surfaces between the base slab and the ground to remain close or open but not to penetrate each other. When fiber composite laminate materials or steel plates are utilized to strengthen the containment, they are also modeled by the 8-node shell elements, which are superimposed to the shell elements of the concrete section.

MATERIAL PROPERTIES AND CONSTITUTIVE MODELS

The materials used in the analysis involve steel reinforcing bar, steel liner plate, strengthening steel plate, concrete and composite material. The constitutive models for steel reinforcing bar, steel liner plate, strengthening steel plate and concrete are available in the ABAQUS material library. The nonlinear constitutive equations for the composite laminate material are coded in FOTRAN as a subroutine and linked to the ABAQUS program.

Steel Reinforcing Bar

The reinforcement used in the containment structure is ASTM A-615 Grade 60 steel with yielding stress σ_y = 413.7 MPa (60 ksi) and elastic modulus E_s = 199.9 GPa. The stress-strain curve of the reinforcing bar is assumed to be elastic perfectly plastic. In ABAQUS, the steel reinforcement is treated as an equivalent uniaxial material smeared through the element section. In order to properly model the constitutive behavior of the reinforcement, the cross sectional area, spacing, position and orientation of each layer of steel bar within each element need to be specified.

Steel Liner Plate and Strengthening Steel Plate

The 0.635 cm (1/4") liner plate inside the dome and cylinder is ASTM SA-285 Grade A or C carbon steel with yield stress σ_y = 165.5 MPa (24 ksi). The 5.08 cm (2") liner plate on the base slab is ASTM SA-516 Grade 70 stainless steel with yield stress σ_y = 260 MPa (38 ksi). The elastic modulus E_s and the Poisson's ratio ν_s of both types of steel liner plates are

assumed to be E_S = 199.9 GPa and ν_S = 0.3. When the liner plate is subjected to biaxial stresses, a von Mises yield criterion $f(\sigma_1, \sigma_2)$ is employed to define the elastic limit, where σ_1 and σ_2 are principal stresses and

$$f(\sigma_1,\sigma_2) = \sqrt{\sigma_1^2 + \sigma_1^2 - \sigma_1\sigma_2} = \sigma_y \tag{1}$$

The response of the liner plate is modeled by an elastic-perfectly-plastic theory with associated flow rule. When the stress points fall inside the yield surface, the behavior of the liner plate is linearly elastic. If the stresses of the liner plate reach the yield surface, the behavior of the liner plate becomes perfectly plastic. Consequently, the liner plate is assumed to fail and can not resist any further loading. When the containment is strengthened by steel plate at the external surface, it is assumed that the strengthening steel plate has the same material properties and constitutive law as the liner plate inside the dome and cylinder.

Concrete

The concrete of the containment structure has a uniaxial compressive strength $f_c^{'}$ = 34.47 MPa (5ksi) and the strain ε_o corresponding to the peak stress $f_c^{'}$ is assumed to be 0.003 [5]. The Poisson's ratio ν_c of concrete is assumed to be 0.2 [6]. The uniaxial tensile strength $f_t^{'}$ of concrete is difficult to measure and is normally taken as approximately [6]

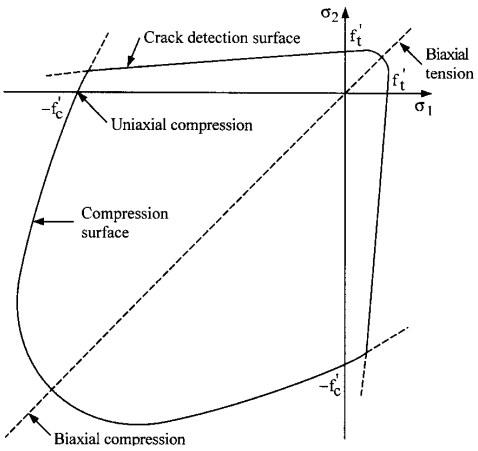

Fig. 3 Concrete failure surface in plane stress

$$f_t^{'} = 0.33\sqrt{f_c^{'}}\ \text{MPa} \tag{2}$$

The initial modulus of elasticity of concrete E_c is highly correlated to its compressive strength and can be calculated from the empirical equation [5]

$$E_c = 4700\sqrt{f_c^{'}}\ \text{MPa} \tag{3}$$

Under different combinations of loading, the failure strengths of concrete are different from that under uniaxial condition. In ABAQUS, a Mohr-Coulomb type compression surface combined with a crack detection surface is used to model the failure surface of concrete (Figure 3). When the principal stress components of concrete are predominantly compressive, the response of the concrete is modeled by an elastic-plastic theory with associated flow and isotropic hardening rule. In tension, once cracking is defined to occur (by the crack detection surface), the orientation of the crack is stored and oriented. Damaged elasticity is then used to model the existing crack [3].

When plastic deformation occurs, a commonly used approach is to relate the multidimensional stress and strain conditions to a pair of quantities, namely, the effective stress σ_c and effective strain ε_c, such that results obtained following different loading paths can all be correlated by means of the equivalent uniaxial stress-strain curve. The stress-strain relationship proposed by Saenz [7] has been widely adopted as the uniaxial stress-strain curve for concrete and it has the following form

$$\sigma_c = \frac{E_c\varepsilon_c}{1 + (R + R_E - 2)(\frac{\varepsilon_c}{\varepsilon_o}) - (2R - 1)(\frac{\varepsilon_c}{\varepsilon_o})^2 + R(\frac{\varepsilon_c}{\varepsilon_o})^3} \tag{4}$$

where $R = \frac{R_E(R_\sigma - 1)}{(R_\varepsilon - 1)^2} - \frac{1}{R_\varepsilon}$, $R_E = \frac{E_c}{E_o}$, $E_o = \frac{f_c^{'}}{\varepsilon_o}$, $R_\sigma = 4$, $R_\varepsilon = 4$

In the analysis, equation (4) is taken as the equivalent uniaxial stress-strain curve for concrete

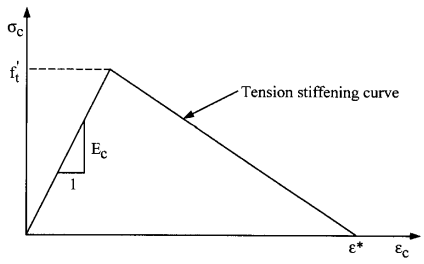

Fig. 4 Tension stiffening model

and approximated by several piecewise linear segments [8]. When cracking of concrete takes place, a smeared model is used to represent the discontinuous macrocrack behavior. It is known that the cracked concrete of a reinforced concrete element can still carry some tensile stress in the direction normal to the crack, which is termed tension stiffening [6]. In this study, a simple descending line (Fig. 4) is used to model this tension stiffening phenomenon. The default value of the strain ε^* at which the concrete stress reduced to zero is $\varepsilon^* = 0.001$ [3]

Fiber Composite Laminate Material

For composite materials, the stress-strain relations in fiber and transverse directions are fairly linear. However, severe nonlinearity in in-plane shear is observed [9] and the nonlinear strain-stress relation for a composite lamina suggested by Hahn and Tsai [9] is adopted in this study, which is given as follows:

$$\begin{Bmatrix}\varepsilon_1\\ \varepsilon_2\\ \gamma_{12}\end{Bmatrix}=\begin{bmatrix}1/E_{11} & -\nu_{21}/E_{22} & 0\\ -\nu_{12}/E_{11} & 1/E_{22} & 0\\ 0 & 0 & 1/G_{12}\end{bmatrix}\begin{Bmatrix}\sigma_1\\ \sigma_2\\ \tau_{12}\end{Bmatrix}+S_{6666}\tau_{12}^2\begin{Bmatrix}0\\ 0\\ \tau_{12}\end{Bmatrix} \tag{5}$$

The value of S_{6666} can be determined by a curve fit to off-axis tension test data [9]. Inverting and differentiating Eq. (5), we can obtain the nonlinear incremental stress-strain relations as

$$\begin{Bmatrix}\Delta\sigma_1\\ \Delta\sigma_2\\ \Delta\tau_{12}\end{Bmatrix}=\begin{bmatrix}E_{11}/(1-\nu_{12}\nu_{21}) & \nu_{12}E_{22}/(1-\nu_{12}\nu_{21}) & 0\\ \nu_{21}E_{11}/(1-\nu_{12}\nu_{21}) & E_{22}/(1-\nu_{12}\nu_{21}) & 0\\ 0 & 0 & 1/G_{12}+3S_{6666}\tau_{12}^2\end{bmatrix}\begin{Bmatrix}\Delta\varepsilon_1\\ \Delta\varepsilon_2\\ \Delta\gamma_{12}\end{Bmatrix} \tag{6}$$

Furthermore, it is assumed that the transverse shear stresses always behave linearly and do not affect the nonlinear behavior of in-plane shear. Among existing failure criteria, the Tsai-Wu criterion [10] has been extensively used in literature and it is adopted in this analysis. Under plane stress conditions, this failure criterion has the following form

$$F_1\sigma_1+F_2\sigma_2+F_{11}\sigma_1^2+2F_{12}\sigma_1\sigma_2+F_{22}\sigma_2^2+F_{66}\tau_{12}^2=1 \tag{7}$$

and $\quad F_1=\dfrac{1}{\overline{X}}+\dfrac{1}{\overline{X}'},\quad F_2=\dfrac{1}{\overline{Y}}+\dfrac{1}{\overline{Y}'},\quad F_{11}=\dfrac{-1}{\overline{X}\overline{X}'},\quad F_{22}=\dfrac{-1}{\overline{Y}\overline{Y}'},\quad F_{66}=\dfrac{1}{\overline{S}^2}.$

The $\overline{X}$, $\overline{Y}$ and $\overline{X}'$, $\overline{Y}'$ are the lamina longitudinal and transverse strengths in tension and compression, respectively, and $\overline{S}$ is the shear strength of the lamina. Though the stress interaction term F_{12} in Eq. (7) is difficult to be determined, it has been suggested by Narayanaswami and Adelman [11] that F_{12} can be set equal to zero for practical engineering applications. Therefore, $F_{12} = 0$ is used in this investigation.

During the numerical calculation, incremental loading is applied to composite plates until failure in one or more of individual plies is indicated according to Eq. (7). Since the Tsai-Wu criterion does not distinguish failure modes, the following two rules are used to determine whether the ply failure is caused by resin fracture or fiber breakage [12]:

(1) If a ply fails but the stress in the fiber direction remains less than the uniaxial strength of the lamina in the fiber direction, i.e. $\overline{X}'<\sigma_1<\overline{X}$, the ply failure is assumed to be resin induced. Consequently, the laminate loses its capability to support transverse and shear stresses, but remains to carry longitudinal stress. In this case, the constitutive matrix of the lamina becomes

$$\begin{Bmatrix}\Delta\sigma_1\\ \Delta\sigma_2\\ \Delta\tau_{12}\end{Bmatrix}=\begin{bmatrix}E_{11} & 0 & 0\\ 0 & 0 & 0\\ 0 & 0 & 0\end{bmatrix}\begin{Bmatrix}\Delta\varepsilon_1\\ \Delta\varepsilon_2\\ \Delta\gamma_{12}\end{Bmatrix} \tag{8}$$

(2) If a ply fails with σ_1 exceeding the uniaxial strength of the lamina, the ply failure is caused by the fiber breakage and a total ply rupture is assumed. In this case, the constitutive matrix of the lamina becomes

$$\begin{Bmatrix}\Delta\sigma_1\\ \Delta\sigma_2\\ \Delta\tau_{12}\end{Bmatrix}=\begin{bmatrix}0 & 0 & 0\\ 0 & 0 & 0\\ 0 & 0 & 0\end{bmatrix}\begin{Bmatrix}\Delta\varepsilon_1\\ \Delta\varepsilon_2\\ \Delta\gamma_{12}\end{Bmatrix} \tag{9}$$

The material properties for fiber composite laminate material used in the analysis are E_{11} = 128 GPa, E_{22} = 11.0 GPa, $G_{12} = G_{13}$ = 4.48 GPa, G_{23} = 1.53 GPa, $S_{6666} = 7.31\times10^{-27}$GPa, $\overline{X}$ = 1450 MPa, $\overline{X}'$ = -1450 MPa, $\overline{Y}$ = 52 MPa, $\overline{Y}'$ = -206 MPa, $\overline{S}$ = 93 MPa, ν_{12} = 0.25.

NUMERICAL ANALYSIS

Ultimate Analysis of Reinforced Concrete Containment without Strengthening Composite Materials

A preliminary ultimate analysis is carried out before any fiber composite laminate materials are used to strengthen the reinforced concrete containment [8]. The containment is subjected to an internal pressure and a dead load due to its own weight. It is assumed that the dead load, w_c, caused by the reinforced concrete [13] is

$$w_c = 23.56\ \text{kN/m}^3\ (150\,\text{lb/ft}^3) \tag{10}$$

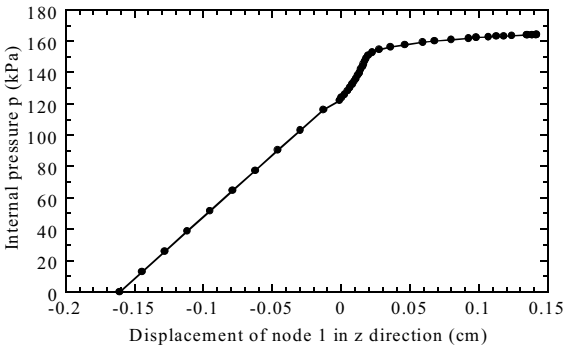

Fig. 5 Load-displacement curve of containment without strengthening materials

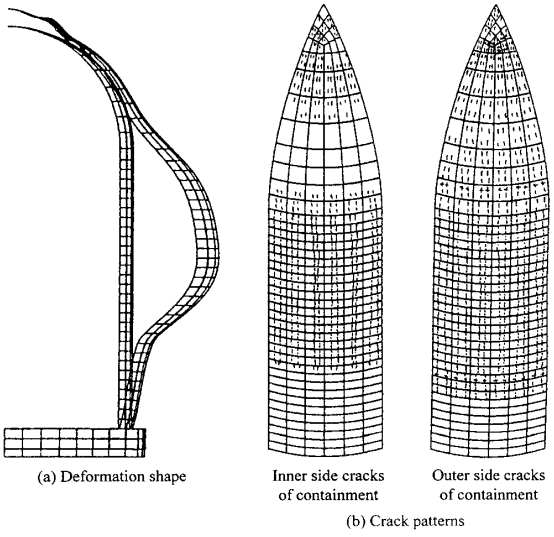

Fig. 6 Failure mode of containment without strengthening materials

Figure 5 shows the internal pressure p verse the displacement of node 1 (at the apex of the containment) in z direction. Due to the dead load, the apex of the containment has an initial downward (negative) displacement at the beginning of the analysis. While the internal pressure is increased, the apex of the containment gradually moves upward up to failure. When the containment is about to fail, there is a significantly ductile deformation taken place at the apex. The ultimate internal pressure p_u of the containment is 164.6 kPa (23.88 psi) which is about 59.2 % higher than the design pressure capacity 103.4 kPa (15 psi) [4].

The deformation shape of the containment under the ultimate internal pressure is shown in Fig. 6a and the crack patterns of the concrete at the inner and outer sides of containment are shown in Fig. 6b. From these figures we can observe that under the ultimate pressure, the base slab still keeps in contact with the ground. Most of the deformations take place in the upper cylinder and dome. In addition, due to stress concentration, cracks are likely to occur near the apex of the dome, the conjunction

of dome and cylinder, and the mid-cylinder location where the thickness changes abruptly.

Ultimate Analysis of Reinforced Concrete Containment Strengthened by Composite Materials or Steel Plates at the Upper Cylinder

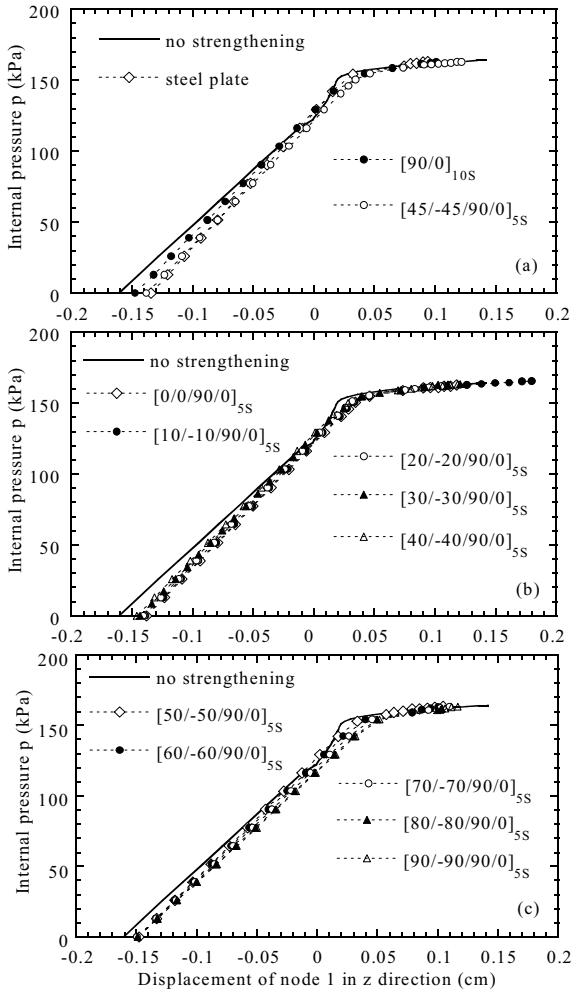

Fig. 7 Load-displacement curve of containment strengthened by steel plates and composite materials at upper cylinder

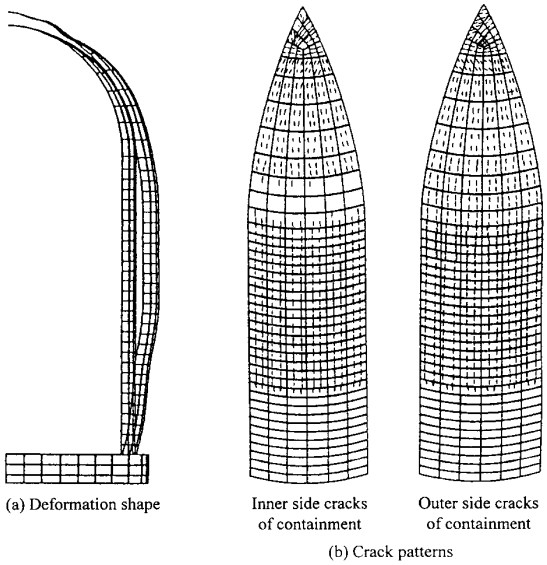

Fig. 8 Failure mode of containment strengthened by $[\pm 45/90/0]_{5S}$ composite material at upper cylinder

From the preliminary study we observe that the upper portion of cylinder has a significant deformation under the ultimate load. This is because the thickness as well as stiffness of the upper cylinder are significantly less than those of the low cylinder. Hence, numerical studies of the containment strengthened by the composite material at the entire upper cylinder, whose thickness is 1.067m (3'-6"), are carried out. The laminate lay-ups for the composite materials are $[90/0]_{10S}$, $[\pm 45/90/0]_{5S}$ and $[\pm\theta/90/0]_{5S}$. The thickness of each lamina is 4 mm and the total thickness of the entire cross section of the composite material is 16 cm. The fiber angle of the lamina is measured counterclockwise (through outward normal direction) from the meridian of containment shell structure. Hence, 0^{o} and 90^{o} would be in the meridian direction and the hoop direction of the shell. For comparison, numerical studies of the containment strengthened by the steel plate are also performed. The thickness of the strengthening steel plate is assumed to be 10 cm.

Figure 7 shows the internal pressure p verse the displacement of node 1 in z direction for the containments strengthened by steel plate or various types of composite laminate lay-ups. All the curves show the similar trend as the one without the use of any strengthening materials and none of them could increase the stiffness as well as the ultimate strength of the containment. Figure 8 shows the failure mode of the containment strengthened by composite materials with $[\pm 45/90/0]_{5S}$ lay-up under the ultimate load stage. Although the deformation of the containment at the upper cylinder (Fig. 8a) is smaller than the unstrengthened one (Fig. 6a), more extensive cracks take place near the apex of the strengthened containment than that of the unstrengthened one. Once the apex fails, the containment can not resist any further loads. Hence, it may be concluded that the apex of the dome is the weakest point of the containment and the use of any

strengthening materials at the upper cylinder will be in vain.

Ultimate Analysis of Reinforced Concrete Containment Strengthened by Composite Materials or Steel Plates at the Dome

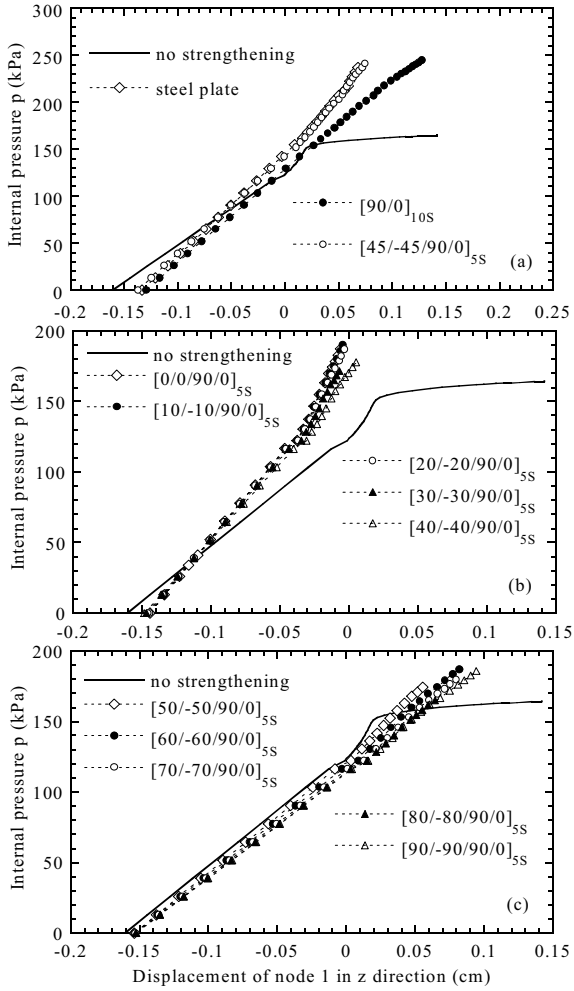

Fig. 9 Load-displacement curve of containment strengthened by steel plates and composite materials at dome

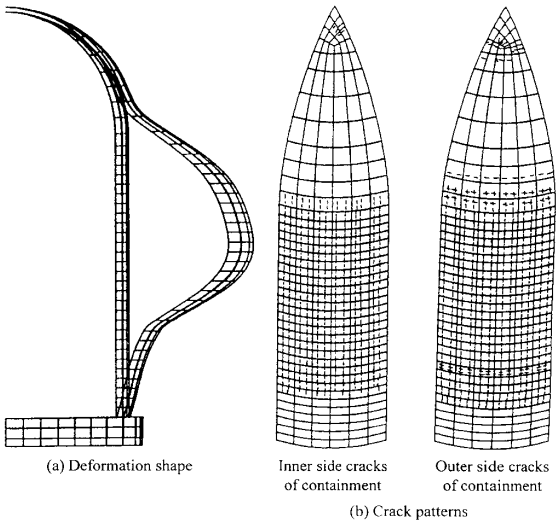

Fig. 10 Failure mode for containment strengthened by $[\pm 45/90/0]_{5S}$ composite material at dome

Base on the results of the previous section, numerical studies of the containment strengthened by the composite materials or steel plates at the entire hemisphere dome are carried out. The laminate lay-ups for the composite materials are the same as before, which are $[90/0]_{10S}$, $[\pm 45/90/0]_{5S}$ and $[\pm\theta/90/0]_{5S}$. The thicknesses of the composite lamina and steel plate are also the same as before.

Figure 9 shows the internal pressure p verse the displacement of node 1 in z direction for the containments strengthened by steel plate or various types of composite laminate lay-ups. Figure 9a shows that the behavior of the containment strengthened by the $[\pm 45/90/0]_{5S}$ composite material is similar to that strengthened by the steel plate. While the containment strengthened by the $[90/0]_{10S}$ composite material has a lower stiffness than the former two, all the strengthened containments have significant higher ultimate strengths than the unstrengthened one. However, these strengthened containments all fail in brittle patterns and no noticeable ductile deformation occurred at the apex. The behaviors of the containments strengthened by the $[\pm\theta/90/0]_{5S}$ composite materials at the dome generally can be separated into two groups. When $0^{o} \le \theta \le 40^{o}$, the employing of composite materials increase the stiffness as well as the ultimate strength of the containment (Fig. 9b). When $50^{o} \le \theta \le 90^{o}$, the employing of composite materials does not increase the stiffness of the containment but only improve the ultimate strength of the containment (Fig. 9c). Nevertheless, all containments strengthened by the $[\pm\theta/90/0]_{5S}$ composite materials also fail in brittle patterns.

Figure 10 shows the typical deformation and crack patterns of the containment strengthened by composite materials with $[\pm 45/90/0]_{5S}$ lay-up under the ultimate load stage. It can be observed that by strengthening the dome, the upper cylinder of the containment undergo more deformation (Fig. 10a) than that without the

use of strengthening materials (Fig. 6a). Although the strengthened dome has much less cracks (Fig. 10b) than the unstrengthened one (Fig. 6b), extensive cracks still take place at the conjunction of dome and cylinder and the mid-cylinder location where the thickness changes abruptly. Hence, it may be concluded that after the dome is strengthened, the upper cylinder becomes the weakest part of the containment.

Ultimate Analysis of Reinforced Concrete Containment Strengthened by Composite Materials or Steel Plates at the Upper Cylinder and Dome

Base on the results of the previous section, numerical studies of the containment strengthened by the composite materials or steel plates at both the upper cylinder and dome are carried out. The laminate lay-ups and thickness for the composite materials are the same as before. The thickness of the strengthening steel plate is reduced to 5 cm.

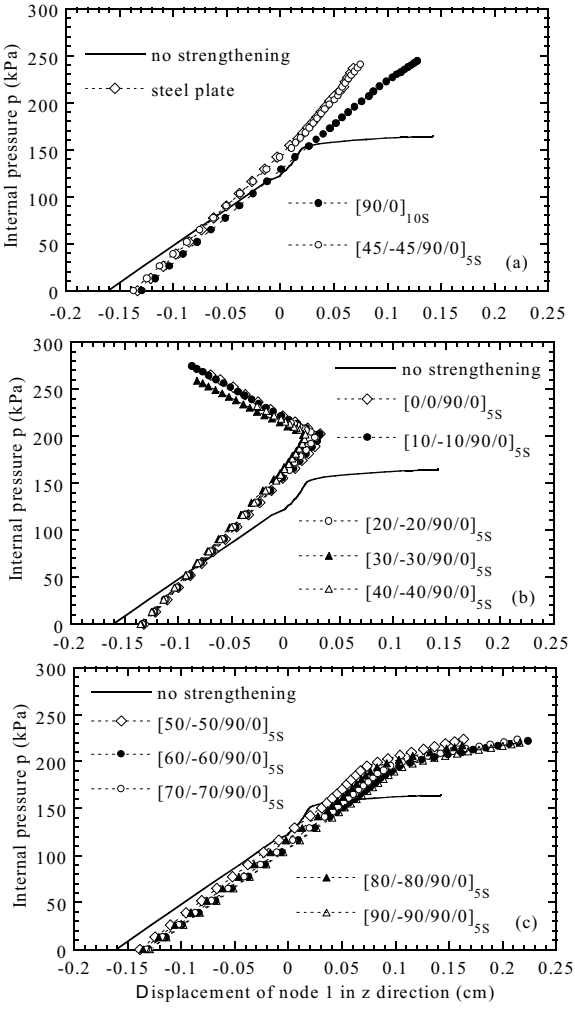

Fig. 11 Load-displacement curve of containment strengthened by steel plates and composite materials at upper cylinder and dome

Figure 11 shows the internal pressure p verse the displacement of node 1 in z direction for the containments strengthened by steel plate or various types of composite laminate lay-ups. Figure 11a is similar to Fig. 9a. It shows that the behavior of the containment strengthened by the $[\pm 45/90/0]_{5S}$ composite material is similar to that strengthened by the steel plate and the containment strengthened by the $[90/0]_{10S}$ composite material has a lower stiffness than the former two. Although the three strengthened containments have significantly higher ultimate strengths than the unstrengthened one, they all fail in brittle patterns and no noticeable ductile deformation occurred at the apex. The behaviors of the containments strengthened by the $[\pm\theta/90/0]_{5S}$ composite materials at the upper cylinder and dome again can be separated into two groups. For $0^{o} \le \theta \le 40^{o}$, the containments exhibit hardening behaviors before the structures fail (Fig. 11b). For $50^{o} \le \theta \le 90^{o}$, the containments exhibit softening behaviors (Fig. 11c) and significantly ductile deformations take place at the apex when the containments are about to fail. Nevertheless, all containments strengthened by the $[\pm\theta/90/0]_{5S}$ composite materials have much higher ultimate strengths than the unstrengthened one. For example, the ultimate strength of the containment strengthened by the $[\pm 50/90/0]_{5S}$ composite materials is 223.7 kPa (32.44 psi), which is higher than the unstrengthened value 164.6 kPa (23.88 psi) by 35.9% and higher than the design pressure capacity 103.4 kPa (15 psi) by 116.3%.

Figure 12 shows the typical deformation and crack patterns of the containment strengthened by composite materials with $[\pm 45/90/0]_{5S}$ lay-up under the ultimate load stage. It can be observed that by strengthening the upper cylinder and dome, the entire containment undergo

more uniform deformation (Fig. 12a) than that without the use of strengthening materials (Fig. 6a). When the containment fails, severe cracks exist near the apex of the dome and the conjunction of dome and cylinder. It seems that the apex of the dome and the conjunction of dome and cylinder are about to fail at the same ultimate load. Due to the ductile behavior and high ultimate strength concerned, it is suggested to employ the $[\pm\theta/90/0]_{5S}$ composite materials with $50^{o} \le \theta \le 90^{o}$ to strengthen the reinforced concrete containment at the upper cylinder and the dome simultaneously.

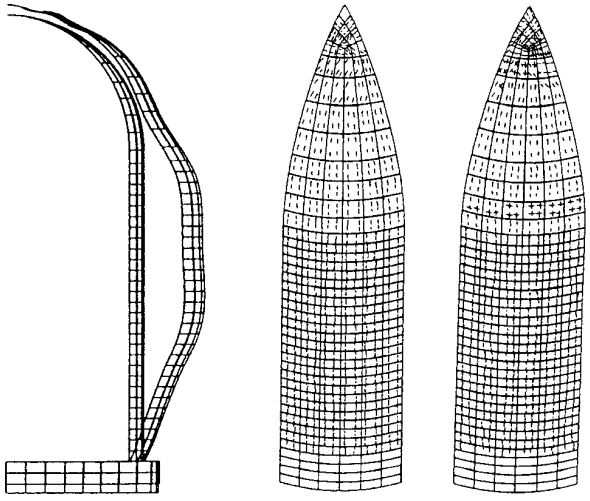

Fig. 12 Failure mode for containment strengthened by $[\pm45/90/0]_{5S}$ composite material at upper cylinder and dome

CONCLUSIONS

In this paper, nonlinear finite element analyses of the reinforced concrete containment at Kuosheng nuclear power plant strengthened by composite materials or steel plates are performed. For simplicity, equipment hatches and penetrations on the containment are not considered. Based on the numerical results from the analyses, the following conclusions may be drawn:

(1) The apex of the dome is the weakest point of the containment structure and the use of strengthening steel plates or composite materials with any types of lay-ups at the upper cylinder will be in vain.

(2) The uses of steel plates or composite materials with $[90/0]_{10S}$ or $[\pm45/90/0]_{5S}$ lay-ups to strengthen the containment at the dome only or at both the upper cylinder and the dome simultaneous generally give higher ultimate strengths than the unstrengthened one. However, due to their brittle failure patterns, the employing of steel plates or composite materials with $[90/0]_{10S}$ or $[\pm45/90/0]_{5S}$ lay-ups to strengthen the containment is not suggested.

(3) The uses of composite materials with $[\pm\theta/90/0]_{5S}$ lay-ups to strengthen the containment at the dome also render higher ultimate strengths and brittle failure patterns and are not suggested.

(4) The uses of $[\pm\theta/90/0]_{5S}$ composite materials with $0^{o} \le \theta \le 40^{o}$ to strengthen the containment at the upper cylinder and dome yield hardening behaviors to the containment and this may not be desired.

(5) The uses of $[\pm\theta/90/0]_{5S}$ composite materials with $50^{o} \le \theta \le 90^{o}$ to strengthen the containment at the upper cylinder and dome yield softening behaviors and ductile deformations to the containment. In addition, the ultimate strengths of these strengthened containments are much higher than the unstrengthened one. Thus, the

employing of the $[\pm\theta/90/0]_{5S}$ composite materials with $50^{o} \le \theta \le 90^{o}$ to strengthen the reinforced concrete containment at the upper cylinder and the dome simultaneously is most recommendable.

ACKNOWLEDGMENT

This research work was financially supported by the Taiwan Power Company via the National Science Council of R.O.C. under Grant number NSC 89-TPC-7-006-016.

REFERENCES

1. Schubbe, J.J. and Mall, S., "Investigation of a Cracked Thick Aluminum Panel Repaired with a Bonded Composite Patch", *Engineering Fracture Mechanics*, 1999. Vol. 63, pp. 305-323.
2. GangaRao, H.V.S. and Vijay, P.V., "Bending Behavior of Concrete Beams Wrapped with Carbon Fabric, *Journal of Structural Engineering (ASCE)*, 1998. Vol. 124, pp. 3-10.
3. Hibbitt, Karlsson & Sorensen, Inc., *ABAQUS Theory Manual and User Manual*, Version 5.8, Providence, Rhode Island, 2000.
4. Taiwan Power Company, *Final Safety Analysis Report*, Kuosheng Nuclear Power Station Units 1 and 2, Volume 5, 1979.
5. ACI Committee 318, *Building Code Requirements for Structural Concrete and Commentary (ACI 318-99)*, American Concrete Institute, Detroit, Michigan, 1999.
6. ASCE Task Committee on Concrete and Masonry Structure. State of the art report on finite element analysis of reinforced concrete. New York: ASCE, 1982.
7. Saenz, L.P., Discussion of "Equation for the stress-strain curve of concrete" by Desayi, P. and Krishnan, S., *ACI Journal*, 1964. Vol. 61, pp. 1229-1235.
8. Hu, H.-T. and Liang, J.-I., "Ultimate Analysis of BWR Mark III Reinforced Concrete Containment Subjected to Internal Pressure", *Nuclear Engineering and Design*, 2000. Vol. 195, pp. 1-11.
9. Hahn, H.T. and Tsai, S.W., "Nonlinear Elastic Behavior of Unidirectional Composite Laminae", *Journal of Composite Materials*, 1973. Vol. 7, pp. 102-118.
10. Tsai, S.W and Wu, E.M., "A General Theory of Strength for Anisotropic Materials", *Journal of Composite Materials*, 1971. Vol. 5, pp. 58-80.
11. Narayanaswami, R. and Adelman, H.M., "Evaluation of the Tensor Polynomial and Hoffman Strength Theories for Composite Materials", *Journal of Composite Materials*, 1977. Vol. 11, pp. 366-377.
12. Rowlands, R.E., "Strength (Failure) Theories and Their Experimental Correlation", in *Failure Mechanics of Composites*, Edited by Sih, G.C. and Skudra, A.M., Elsevier Science Publishers, The Netherlands, 1985, pp. 71-125.
13. Wang, C.-K. and Salmon, C.G., *Reinforced Concrete Design*, Sixth Edition, Chapter One, Addison Wesley, New York, 1998.